

HybNet: A Hybrid Deep Learning - Matched Filter Approach for IoT Signal Detection

Kosta Dakic*, *Graduate Student Member, IEEE*, Bassel Al Homssi, *Member, IEEE*,
 Margaret Lech, *Member, IEEE*, and Akram Al-Hourani*, *Senior Member, IEEE*,

Abstract—Random access schemes are widely used in IoT wireless access networks to accommodate simplicity and power consumption constraints. As a result, the interference arising from overlapping IoT transmissions is a significant issue in such networks. Traditional signal detection methods are based on the well-established matched filter using the complex conjugate of the signal, which is proven as the optimal filter under additive white Gaussian noise. However, with the *colored* interference arising from the overlapping IoT transmissions, deep learning approaches are being considered as a better alternative. In this paper, we present a hybrid framework, *HybNet*, that switches between deep learning and match filter pathways based on the detected interference level. This helps the detector work in a broader range of conditions, optimally leveraging the matched filter and deep learning robustness. We compare the performance of several possible data modalities and detection architectures concerning the interference-to-noise ratio, demonstrating that the proposed HybNet surpasses the complex conjugate matched filter performance under interference-limited scenarios.

Index Terms—Internet-of-Things, LoRa, deep learning, chirp spread spectrum, convolutional neural network, matched filter, signal detection, interference.

I. INTRODUCTION

The growth of Internet-of-Things (IoT) technologies is anticipated to play a significant role in the future of societies by facilitating the connectivity between sensor devices and Internet cloud services. According to a report from Ericsson, it estimates over 5 billion cellular IoT devices connections by 2025 [1]. For wireless IoT devices, this increase would further congest spectrum resources and increase interference. This is already evident in the license-free industrial, scientific, and medical (ISM) band [2] since this band is available to the public and does not require paid licensing.

Radio frame reception is typically based on matched filter receiver architecture, where the signal is compared, or *matched*, to a known template. This method is proven to be optimal under additive white Gaussian noise (AWGN) conditions [3]. In centrally controlled networks, the base station, e.g., gNB in 5G, orchestrate the access to the spectral resources by employing a multiple-access technique such as time-division multiple access (TDMA), frequency-division multiple access (FDMA), code-division multiple access (CDMA), and orthogonal frequency-division multiple access (OFDMA). These access techniques are required to alleviate the co-channel interference. Nevertheless, such techniques require significant overhead, adding complexity

*Corresponding authors: K. Dakic and A. Al-Hourani, with the School of Engineering, RMIT University, Melbourne, VIC 3000. E-mail: kosta.dakic@ieee.org, akram.hourani@rmit.edu.au.

to the protocol stack. Thus, typical license-free IoT networks employ random access techniques to simplify the protocol stack because a complex access technique would not be efficient in the first place given the interference originating from other co-existing systems in the same band.

Efficient signal detection is crucial for Low power wide area networks (LPWAN) technologies, which are receiving increasing attention due to the increasing use of IoT applications. LPWANs can achieve long-distance communication while maintaining low-power consumption, which is indeed at the cost of a reduced bit rate. In a license-free spectrum, LPWAN network performance is typically interference-limited in urban environments, while it becomes noise-limited in rural and remote locations. A prominent LPWAN technology is LoRaWAN, adopted by the LoRa Alliance [4]. LoRaWAN typically uses an unslotted ALOHA-based protocol, allowing multiple IoT devices to transmit without coordination. As such, the transmitted signals are prone to packet collisions which significantly reduces the performance [5]–[9]. LoRaWAN utilizes the LoRa modulation technique, which is based on chirp spread spectrum (CSS) modulation spreading the signal energy over a wider bandwidth to combat narrowband interference [8]. Furthermore, the time-spreading of the transmission can be controlled using a parameter called *spreading factor* (SF), which increases the energy at the receiver without the need to transmit at a higher RF power. Aside from potential narrowband interference, LoRa-to-LoRa induced interference significantly degrades the performance, especially when using the same SF.

The rapid evolution of neural networks (NN), particularly deep learning (DL) methods, have shown great potential for signal detection [10]–[13]. The main appeal of DL signal detection is its strength against non-linearities [14]. Notably, the Convolutional Neural Network (CNN) has been utilized to classify stochastic signals such as in image classification [15], which is not practically possible using deterministic methods such as the matched filter.

This paper presents a new framework, *HybNet*, that switches between matched filter detection and a proposed deep learning detector, where the switching is performed based on the interference level. Our framework harnesses the benefits of both the matched filter's ideal performance under AWGN noise-limited scenarios and the improved performance of the proposed DL detector in LoRa-to-LoRa interference. Additionally, we explore three different input data modalities for the DL-based detection; (i) time-domain (I/Q samples), (ii) time-frequency domain (spectrogram), and (iii) frequency domain (spectrum). Results show that the proposed DL-detectors outperform

traditional coherent and noncoherent detection performance in non-Gaussian interference scenarios. In order to evaluate the proposed framework at different interference/noise mixtures, we vary the interference to noise ratio (INR) and obtain the corresponding bit-error rate (BER). Accordingly, the overall BER performance results indicate that the proposed DL-based detectors can significantly improve LoRa detection performance for LoRa symbols under high interference scenarios. The contribution of this work is summarized as follows,

- It develops a novel hybrid framework comprising of a CNN interference detector that switches between two different pathways: (i) a coherent detector and (ii) a CNN signal detector.
- It presents a method for creating a dataset of LoRa symbols in three modalities: the time domain, time-frequency domain, and frequency domain representations with AWGN impairment and LoRa interference for training CNN networks for detection.
- It provides a comparison framework for evaluating symbol detection under different interference scenarios and input data modalities.

The rest of this paper is organized as follows. A literature review is presented in Section II. An overview of the systems model which utilizes LoRa modulation along with LoRa emulation and dataset creation is covered in Section III. Section IV discusses the DL detection architectures utilized in this paper. Section V discusses the results obtained from the experiments. Finally, Section VI concludes the paper.

II. BACKGROUND AND RELATED WORK

Interference is a significant issue that hinders efficient packet reception, particularly in the license-free spectrum bands. In such bands, different users and systems access the spectrum without resource coordination. Thus, extensive literature is available on the Cognitive Radio (CR) concept. CR senses spectrum occupancy and devises a spectrum access plan to mitigate co-channel interference [16]. However, the efficiency of CR is limited to the predictability of the spectrum. As such, random-access networks severely reduce such capacity. Also, CR requires additional electric power for spectrum sensing, which is not ideal for battery-operated devices [17]. In all cases, CR has not been adopted in practical IoT communication systems due to these limitations, among others. Another technique to increase the capacity of a system with interference from another signal is to utilize successive interference cancellation (SIC), initially proposed in [18]. In SIC, signals coming from different users are successively decoded, each decoded signal is subtracted from the received signal, and the cycle is repeated. SIC is utilized in non-orthogonal multiple access (NOMA) for the next generation of wireless communications. However, the channel gains of all users should be known by the base station (BS) for correct decoding of the superimposed signals, which entails additional overhead [19].

In the LoRa modulation method, transmissions with different SFs demonstrate a certain level of orthogonality, as the cross-energy between two non-synchronized LoRa packets is reduced [20]. However, collisions of inter-SF signals would

in-practice still cause packet loss, as shown in [8], [20]–[22]. To add to the problem, the collision of LoRa signals with the same SF is even more severe, thus requiring a higher signal to interference plus noise ratio (SINR) to be successfully detected [8]. To address same-SF interference, authors in [23] propose the use of allocating different SFs. However, while the proposed method improves the overall throughput performance, LoRa interference still poses a challenge. Recent research has also shown how coherent detection enhances the performance in same-SF interference scenarios, where theoretical approximations and Monte Carlo simulations are shown in [22]. However, the work concentrates on same-SF interference as inter-SF interference has a broader spectrum band and lower power spectral density after dechirping [22]. Additional references on investigating the BER performance of traditional LoRa receivers under interference can be found in [24] and [9]. Another research work has also explored theoretical LoRa BER performance for conventional receivers under AWGN and fading channel conditions in [25].

Machine learning (ML) methods, with a focus on DL, have been recently applied in the research field of wireless communications, including works on automatic modulation recognition (AMR) [16], [26], occupancy detection in the license-free band [27], [28], optimization of interference management algorithms [29], among many more applications, which are further reviewed in [14] for the physical layer of communications, and in [30] for higher layers. These works show that DL is a promising tool in the research area of wireless communications. Our previous work in [10] explored the use of DL-based detection techniques with CNN models for the LoRa modulation scheme under AWGN, time offset, and frequency offset conditions. Another research work that utilizes DL sequence detector networks can be found in [11], constructing a sliding bidirectional recurrent neural network (SBRNN). The SBRNN can take in information from previous symbols, unlike symbol-by-symbol detectors, to combat inter-symbol interference (ISI) for non-LoRa signals. Another advantage of DL-based detectors is that they do not need channel state information (CSI) which is further demonstrated in [12] proposing a detection method based on the generative adversarial network (GAN). The work further develops the DL-based symbol detector presented by [13], presenting a model-based approach that uses DL to learn the log-likelihoods and performs Viterbi detection. In addition to solid detection performance, the research work also proposes a method to train in real-time and adapt to time-varying channels.

Another research area on utilizing DL in communications systems is to emulate end-to-end physical layer using an autoencoder (AE), called the channel AE [31]. The idea is to replace the transmitter with an encoder and the receiver as the decoder, which is realized with DL [32]. The channel AE assumes the complete communication procedure, including detection. Authors in [31] present a channel AE with a pre-known theoretical channel model, further optimized to combat common channel impairments, such as AWGN, unknown time and rate of arrival, delay spread, and carrier frequency and phase offset. However, when the communication channel is more complex, the performance is worse than in [33], which

does not assume the channel model in advance.

For non-Gaussian interference, research work showing DL-based channel estimation and signal detection is proposed in [34] for OFDM systems, showing robustness to non-linear channel impairments, interference, and comparable BER performance to traditional detection methods. In [35], the authors investigate DL-based detection using a CNN and a fully connected NN on symbols with QPSK and 8PSK modulation schemes and are superimposed by co-channel interference. Authors in [36] show a DL-based approach for detecting MIMO signals with correlated interference using a maximum likelihood detector and a DL network to predict and remove local correlation among the noise in different symbols. Nonetheless, there seems to be no other research work investigating the issue of LoRa with the same technology interference utilizing DL-based detection.

III. IOT SIGNAL MODEL

As a prominent application of an IoT signal, we utilize the popular LoRa modulation scheme. This section explains the general structure of a LoRa symbol and outlines the two main traditional detection methods. We then cover the dataset creation methodology as used to train the deep learning networks.

A. LoRa Modulation

LoRa CSS modulation is based on linear cyclic chirping within a bandwidth B . Each chirp encodes one symbol with a duration T_s . The bandwidth in LoRaWAN can take one of the following values as $B \in \{125, 250, 500\}$ kHz and the chirp rate of the symbol is controlled by the SF, where the SF in LoRa has a range of $SF \in \{7, 8, 9, 10, 11, 12\}$, as per the LoRaWAN standard. The SF can also be used to calculate the range of possible symbol values that a symbol can encode, which is represented as $M = 2^{SF}$. We follow the same notation as in [7] and [10] to describe LoRa signal modulation, where a single symbol is represented as,

$$s_k(t) = \exp \left(j2\pi \int_0^t \left[(\beta x + \zeta_k)_{\text{mod}_B} - \frac{B}{2} \right] dx \right), \quad (1)$$

where ζ_k is the frequency representing the symbol value as follows,

$$\zeta_k = m_k \Delta_f, \quad (2)$$

where m_k is the data symbol value $m_k \in \{0, 1, \dots, M-1\}$, k is the symbol's index, and Δ_f represents the frequency step between the shifts. The frequency step in LoRa is selected to be equal to the symbol rate itself B/M . β represents the chirp rate given by,

$$\beta = \frac{f_{\text{high}} - f_{\text{low}}}{T_s} = \frac{B}{T_s}, \quad (3)$$

where $f_{\text{low}} = f_c + \frac{B}{2}$ and $f_{\text{high}} = f_{\text{low}} - \frac{B}{2}$ are the lower and upper frequency bounds of the chirp respectively around the carrier f_c . Thus, a sequence of symbols can be written as,

$$x(t) = \sum_{k=1}^K s_k(t - kT_s), \quad (4)$$

where K is the total number of symbols contained within a message.

B. Conventional LoRa detection

Typical detection of LoRa symbols can be divided into two steps; (i) The symbol is dechirped with the same chirping rate in order to convert the received symbol into a single tone, accordingly the sequence of symbols will manifest as a Multiple Frequency Shift Keying (MFSK), (ii) Then in the second step the symbol is detected.

To dechirp the signal, each symbol in the received LoRa waveform is multiplied by an inverted chirp with zero frequency shift. The dechirping symbol train is represented as follows,

$$s^*(t) = \sum_{k=1}^K \exp \left(j\pi B(t - kT_s) - j2\pi\beta(t - kT_s)^2 \right), \quad (5)$$

In an ideal channel, each received LoRa symbol can then be dechirped as follows,

$$z(t) = \sum_{k=1}^K \exp \left(j2\pi\zeta_k(t - kT_s) \right), \quad (6)$$

which is a sequence of single tones, each tone with frequency offset ζ_k corresponding to the value of the symbol. This is a typical MFSK signal. Accordingly, we can use conventional MFSK detection methods to detect the symbols. Two main approaches are utilized; (i) noncoherent detection when phase information is not available, and (ii) coherent detection when an actual in-phase and quadrature path are used in the receiver. The traditional detection methods are detailed as follows,

1) *Noncoherent detection*: For non-coherent detection, after dechirping, the square-law (envelope) detector can be used [3] and then the absolute maximum is taken as follows,

$$\hat{m}_{\text{ncoh}} = \underset{k}{\text{argmax}} \left| \int_0^\infty z(t) S_k(t - \tau) d\tau \right|, \quad (7)$$

where the dechirped signal is denoted as $z(t)$. $S_k(t)$ represents the possible dechirped realizations of $z(t)$, where k is an integer representing all symbol possibilities $k = \{0, 1, \dots, M-1\}$. Equivalently, the fast Fourier transform (FFT) can be employed, where the maximum magnitude denotes the symbol estimate \hat{m}_{ncoh} as follows,

$$\hat{m}_{\text{ncoh}} = \left\lfloor \frac{1}{\delta_f} \underset{f}{\text{argmax}} |Y(f)| \right\rfloor, \quad (8)$$

where $Y(f) = \text{FFT}\{y(t)\}$ denotes the FFT of the received FSK signal and $\lfloor \cdot \rfloor$ represents the rounding function. This method achieves the same performance as by correlating with all possible values, at much less complexity. However, non-coherent detection comes at the cost of higher BER compared to coherent detection in AWGN environments.

2) *Coherent detection*: Optimal detection of a LoRa symbol in AWGN environments can be achieved using coherent detection. Coherent detection is executed by correlating the dechirped signal with all possible frequency shifts, then the frequency shift with the largest real valued output denotes the symbol value. MF of an MFSK LoRa symbol is shown as follows,

$$\hat{m}_{\text{coh}} = \underset{k}{\text{argmax}} \text{Re} \left[\int_0^\infty y(t) w_k(t - \tau) d\tau \right], \quad (9)$$

where $w_k(t) = \exp(j2\pi k\Delta_f t)$ represents a set of harmonics. Like with noncoherent detection, coherent detection can be efficiently implemented as the FFT [37], as follows,

$$\hat{m}_{\text{coh}} = \left| \frac{1}{\delta_f} \underset{f}{\text{argmax}} \text{Re}[Y(f)] \right|. \quad (10)$$

While coherent detection is optimal in AWGN environments, since only the real part is used for detection, phase impairments cause a loss in information [37].

C. Dataset Creation

To emulate the target LoRa symbols, we use an open-source MATLAB emulator [7], [38] which was previously developed by our team. The generated LoRa signal is an I/Q waveform, with a SF = 7, and a $B = 125$ kHz. A randomly generated LoRa message consisting of the symbol sequence vector $M = \{m_1, m_2, \dots, m_n\}$ is utilized to create the waveforms. For the training and detection process, a sequence is picked up arbitrarily to represent the *target* signal and give it a controlled power of p_s , while another signal is picked up to represent the *interference*. In addition to the interference, the received target signal is further impaired with a Gaussian noise process having a controlled power. We denote controlled interference power as p_I and the noise power as σ^2 . The INR is denoted as α , and the SINR is denoted as γ ,

$$\alpha = \frac{p_I}{\sigma^2}, \quad \gamma = \frac{p_s}{p_I + \sigma^2}. \quad (11)$$

Since the performance is only related to the INR and SINR, we normalize the interference and noise power with respect to the target LoRa signal power, i.e., $p_s = 1$. Accordingly, the stored emulated received waveform is comprised of three parts; (i) the target LoRa signal, (ii) the interference, (iii) the AWGN noise, as follows,

$$r(t) = \underbrace{x(t)}_{\text{Signal}} + \underbrace{\sqrt{\frac{\alpha}{\gamma + \alpha\gamma}} x_I(t - \tau)}_{\text{Interference}} + \underbrace{\sqrt{\frac{1}{\gamma + \alpha\gamma}} n(t)}_{\text{AWGN}}, \quad (12)$$

where $x(t)$ is the target LoRa baseband signal, $x_I(t)$ is the interfering baseband LoRa signal with a time shift of τ , and $n(t) \sim \mathcal{CN}(0, 1)$ is the complex zero-mean AWGN.

The complex baseband signal is cropped into LoRa symbols, where each target symbol is synchronized in time. The cropped symbols are sampled at $f_s = 125$ kHz. Each training symbol is labeled and can be represented as follows,

$$T = \{(H_1, m_1), (H_2, m_2), \dots, (H_k, m_k)\}, \quad (13)$$

where H_k is the type of representation of the symbol, either in I/Q, STFT, or FFT, depending on the network that is to get trained (one of the three datasets, shown in Fig 1), and m is the symbol label. Note that this work concentrates on detecting target LoRa symbols with SF = 7. Training to detect symbols with a SF greater than SF7 requires that for every increment of SF, the size of the training dataset be cumulatively doubled. The training dataset must increase due to the number of classes increasing according to the number of possible symbol values that a symbol can encode, which is equal to 2^{SF} .

TABLE I
NOTATIONS AND SYMBOLS

Parameter	Symbol	Value
Spreading factor	SF	7
Bandwidth	B	125 kHz
Sampling rate	f_s	125 kHz
Samples per symbol	N	128
Frequency offset	ζ	-
Chirp slope	β	-
Symbol time	T_s	1.024 ms
Noise power spectral density	N_o	-
Symbol	m	-
Discrete frequency step	δ_f	976.56 sym/s
Average noise power	σ^2	-
LoRa symbol	$s_k(t)$	-
Dechirping LoRa signal	$s^*(t)$	-
Dechirped LoRa signal	$z(t)$	-
FSK signal FFT	$R(f)$	-
Non-coherent FSK symbol	$\hat{m}_{\text{n-coh}}$	-
Coherent FSK symbol	\hat{m}_{coh}	-
INR	α	-
SINR	γ	-
Target signal power	p_s	1
Interference signal power	p_I	-
Number of training frames	-	110,000
Number of validation frames	-	30,000
Labeled Lora dataset	T	-
STFT window type	-	Hamming
Points per FFT window for the STFT	W	64
STFT window overlap	L	63
Symbol STFT	X_{STFT}	-
I/Q modality network input	R_k	-
Time-frequency modality network input	X_k	-
Spectrum modality network input	Y_k	-

If the training dataset size is not increased to accommodate the SF change, the BER performance would also decrease. Consequently, the training time would be much longer, and the network complexity would also need to increase due to the increased size of the input data. Additionally, we investigate only a single interfering LoRa signal, where the DL-based detectors are trained with interfering LoRa signals with a SF of 7 to 12. For our DL-based models to detect LoRa symbols with more than one Lora interferer, the training datasets would need to have LoRa frames with multiple interfering LoRa signals. An illustration of the dataset creation is depicted in Fig 1. Note that the process of storing each signal to be trained for the three different data modality networks is covered in subsection IV-A.

IV. DEEP LEARNING DETECTION

The elements that make up the CNNs used in this paper are as follows: (i) convolutional layers interlaced with (ii) max-pooling layers and (iii) batch normalization layers. The convolutional layer performs the convolution operation on the input with a kernel. The window of the kernel slides across the input data with a unity stride in the proposed networks. The output is then multiplied by an activation function, where the Rectified Linear Unit (ReLU) is utilized. Note that the ReLU function is linear for positive inputs and gives zero for negative inputs. In our work, each convolutional layer is followed by a batch normalization layer, which normalizes the mean and variances of the convolutional layer output, which speeds up training. A max-pooling layer precedes the final

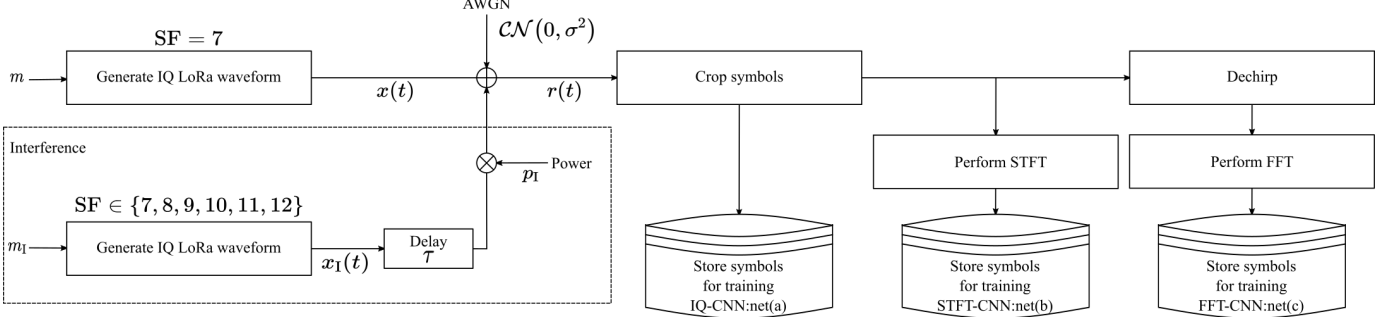


Fig. 1. Dataset generation process for training each CNN.

batch normalization layer in the network, which down-samples the data by taking the maximum value in each max-pooling filter. The output is then passed into a fully connected layer that uses a Softmax activation function that outputs an l -length vector of scores summing to 1, where l is the number of classes. Finally, a classification layer assigns the classes according to the probabilities.

A. Data Modalities

In this section, we explain the three different data modalities that could be used for detecting LoRa signals:

1) *I/Q Modality*: The first model is constructed with the time-domain in-phase and quadrature (I/Q) samples. The model takes in the complex input signal represented as the real part,

$$R_k^I = \text{Re}[r_k(1), r_k(2), \dots, r_k(N)], \quad (14)$$

and the imaginary part,

$$R_k^Q = \text{Im}[r_k(1), r_k(2), \dots, r_k(N)], \quad (15)$$

where for each k -th symbol there are N temporal samples. The samples are then arranged into two 1D vectors to be used in the DL network as follows,

$$R_k = \begin{bmatrix} R_k^I \\ R_k^Q \end{bmatrix}. \quad (16)$$

2) *Time-Frequency Modality*: In the second modality, we convert the time domain samples into a spectrogram using short-time Fourier transform (STFT). STFT works by taking segments, *strides*, of the time domain signal and converting each one using FFT. After that, the FFT vectors are combined in a 2D matrix representing the spectral change across time. In such representation, a linear chirp, for example, will appear as a straight line. The STFT matrix is expressed as follows,

$$X_{\text{STFT}}(\omega, p) = \sum_{n=0}^{N-1} r_k(n)g(k - pL)e^{-j\omega k}, \quad (17)$$

where $X_{\text{STFT}}(\omega, p) \in \mathbb{C}^{W \times \frac{N-L}{W-L}}$. $r_k(\cdot)$ denotes the captured sample of a cropped discrete-time LoRa baseband symbol. A Hamming windowing function is denoted by $g(\cdot)$ with a length of W and L is the overlap length between each Discrete Fourier

Transform (DFT). The parameters chosen for the STFT are outlined in Table I.

The samples are then arranged into two 2D vectors to be used in the DL network as follows,

$$X_k = \begin{bmatrix} \text{Re}[X_{\text{STFT}}] \\ \text{Im}[X_{\text{STFT}}] \end{bmatrix}. \quad (18)$$

3) *Spectrum Modality*: The third modality is based on the frequency domain, where only the real components of an FFT of a dechirped LoRa symbol are used. The input signal can be represented as follows,

$$Y_k = \text{Re}\{\text{FFT}[y_k(1), y_k(2), \dots, y_k(N)]\}, \quad (19)$$

where $y_k(\cdot)$ is the dechirped LoRa symbol.

B. Hybrid Architecture: *HybNet*

The HybNet architecture switches between two different detection branches; (i) the FFT-CNN as referred to in Fig. 3), and (ii) coherent detection. This architecture is designed to incorporate the best performance in AWGN and in co-channel interference conditions. Thus, a supervisory interference detector CNN is utilized to make the decision whether to pass the signal to the first branch or the second. Note that this supervisory network is trained with a similar dataset used to train the FFT-CNN branch. However, the LoRa symbols are labeled with either one of two possible classes; (i) *Noise only* or (ii) *Interference only*. If the interference detector network classifies the received baseband LoRa symbol as “Noise only”, indicating the received symbol does not have LoRa interference or the gain corresponding to the interfering LoRa signal is less than the gain of the target. Consequently, the received symbol is passed to be purely detected by the coherent detector (outlined in subsection III-B2). Suppose the interference detector network classifies the received baseband LoRa symbol as “LoRa interference” whereby the gain corresponding to the LoRa interference is greater than the gain corresponding to the target symbol. In that case, the received symbol is passed to the FFT-CNN branch. An illustration of the utilized switching architecture is shown in Fig. 2.

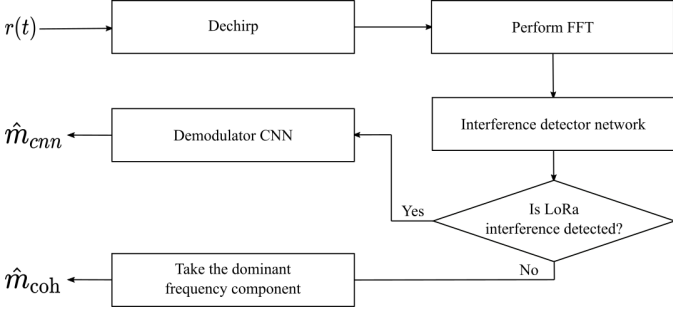


Fig. 2. Illustration of the proposed HybNet architecture switching between deep-learning branch and a matched filter-branch based on the interference to noise ratio.

C. CNN Setup Description

Three different CNN networks were designed to cater to the three data modalities explained in Section IV-A, and this is because they both input demotions and contents are different. For each network of the three networks, we utilize a Bayesian optimizer to choose the network's hyperparameters. Bayesian optimization is a more efficient method for selecting hyperparameters compared to search methods such as brute-force, grid search, and random search [39]. The hyperparameters are chosen to be optimized (i) the number of convolutional layers, (ii) convolutional filter size, (iii) initial learning rate, and (iv) the dropout rate. The consequent network dimensions are summarized in Table II. The CNN architectures are also illustrated in Fig 3, showing the input format to each network. The initial learning rate of the different architectures is optimized to 0.015, 0.001, and 0.0056 for the IQ-CNN, STFT-CNN, and FFT-CNN, respectively. Additionally, considering the simple classification task, the network architectures are shallow.

The interference detector network was manually optimized for the hard switching architecture since high accuracy is achieved with a straightforward network. A simple two-layer CNN was used, which is described in Table III. All the networks were trained with stochastic gradient descent with momentum (SGDM) over 60 epochs. The training parameters for all the networks discussed in this paper are outlined in Table IV.

V. SIMULATION RESULTS AND DISCUSSION

This section presents the performance benchmarking of the different architectures based on the BER indicator. A Monte-Carlo simulation of both *same-SF* interference (SF7 on SF7) and *inter-SF* interference (SF8 on SF7) is performed. The performance is investigated for a variable level of INR. A lower INR value indicates a noise-dominant scenario, while a higher value indicates a more interference-dominant scenario. We have not presented BER plots for varying SINR because BER is known to enhance with the increasing SINR, a consistent trend in any detection algorithm. As such, we pick a transitional SINR where INR significantly impacts the BER performance, without loss of generality, so we fix the SINR at value $\gamma = -15\text{dB}$.

A. Detection Performance

The BER performance of the DL-based techniques, along with traditional coherent and noncoherent methods, is depicted in Fig. 5. DL-based methods outperform conventional detectors in interference-limited scenarios while maintaining a better performance than noncoherent detection in noise-limited scenarios. Furthermore, we put them to the test when we check the performance for a same-SF LoRa interferer, with SF7 in Fig. 4. The figure shows that the trend holds especially for FFT-CNN, which produces good performance under both noise-limited and interference-limited scenarios.

In Fig. 4, we show the BER results for detection of target LoRa symbols with SF7 and an interference LoRa signal also with SF7. From the plot, it can be observed that FFT-CNN outperforms other detectors in an interference-limited scenario. However, as expected, the coherent detector has the best performance in a noise-limited scenario.

As such, the DL-based detection techniques outperform the conventional detection techniques for LoRa-on-LoRa interference scenarios when the power of the interfering signal is higher than the power of the target signal. This is because the DL network is trained on LoRa interference scenarios, so the DL-based techniques learn to discern the interference from the target LoRa signal.

The performance of HybNet is depicted in Fig. 6, Fig. 7 for SF7 and SF8 interference, respectively. It can be clearly seen how the proposed HybNet architecture can effectively switch between the coherent detector and the FFT-CNN branches and thus follows the optimal performance in both noise-limited and interference-limited scenarios. The efficient switching indicates that the interference detector network can accurately detect LoRa interference.

B. Complexity Analysis

We further analyze the training time and detection time of the three main architectures discussed in this paper, the IQ-CNN, STFT-CNN, and the FFT-CNN, in addition to the performance of HybNet. We utilize MATLAB for prepossessing and for DL. The system used for the experimentation has a 16 logical core Intel Xeon at 3.2 GHz CPU and an Nvidia Quadro 4000 GPU. Fig. 8 shows the time performance of the networks, including the accuracy as the number of convolutional layers increases. The results show that at a convolutional depth of one layer, none of the architectures can learn from the input data. At the optimized depths chosen by Bayesian optimization, shown in Fig. 3, the networks have the optimal classification accuracy, thereby validating the optimized architecture. The figure also shows the training time for each architecture, where the STFT-CNN takes the longest to train since the input is a 2D STFT with two channels compared to the 1D input used by the IQ-CNN and FFT-CNN. Finally, the figure shows the detection time required to identify a packet consisting of 20 symbols. These results show that the FFT-CNN has the most desirable performance in classification accuracy, training time, and the lowest detection time. It is clear that the detection time can be controlled by reducing the number of convolutional

TABLE II
CNN NETWORK SUMMARY

Layer	Shape			Parameter
	IQ - CNN Net(a)	S - CNN Net(b)	FFT - CNN Net(c)	
Input Shape	$128 \times 1 \times 2$	$64 \times 65 \times 2$	$128 \times 1 \times 1$	-
Convolutional Layer 1	$8, 5 \times 1$	$9, 7 \times 7$	$8, 19 \times 1$	ReLU
Batch Normalization Layer 1	-	-	-	-
Convolutional Layer 2	$8, 5 \times 1$	$9, 7 \times 7$	$8, 19 \times 1$	ReLU
Batch Normalization Layer 2	-	-	-	-
Convolutional Layer 3	$8, 5 \times 1$	$9, 7 \times 7$	$8, 19 \times 1$	ReLU
Batch Normalization Layer 3	-	-	-	-
Convolutional Layer 4	$8, 5 \times 1$	-	$8, 19 \times 1$	ReLU
Batch Normalization Layer 4	-	-	-	-
Max pooling Layer	2×1	2×1	2×1	-
Dropout Layer	0.36	0.37	0.24	-
Fully Connected	128	128	128	Softmax

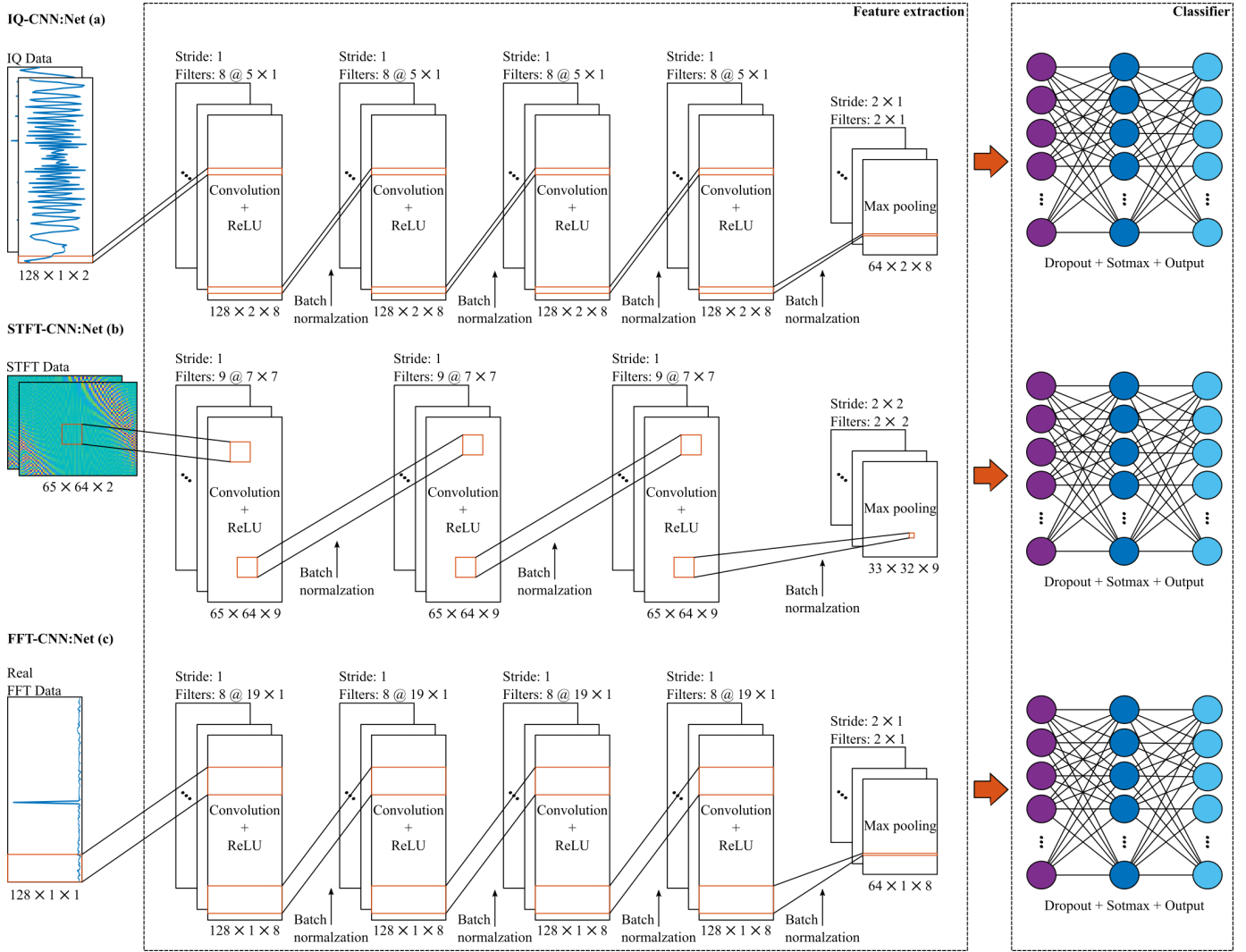


Fig. 3. Illustration of all three DL-based detector models used in this paper.

layers. However, reducing the number of convolutional layers comes at the cost of reduced overall classification accuracy.

For HybNet, the training time is the sum of the FFT-CNN

and the interference detector network, which is ≈ 5 minutes on the used platform. So the overall training time for the HybNet is ≈ 30 minutes. The average detection time per a 20

TABLE III
INTERFERENCE DETECTOR NETWORK

Layer	Shape	Parameters
Input Shape	$128 \times 1 \times 1$	-
Convolutional Layer 1	$4, 19 \times 1$	ReLU
Batch Normalization Layer 1	-	-
Convolutional Layer 2	$4, 19 \times 1$	ReLU
Batch Normalization Layer 2	-	-
Max pooling Layer	2×1	-
Dropout Layer	0.30	-
Fully Connected	2	Softmax

TABLE IV
TRAINING OPTIONS

Parameter	Value
Optimizer	SGDM
Momentum	0.9
Epochs	60
Learning rate drop schedule	40
Learning rate drop factor	0.1
Mini-batch size	256
L2 regularization	0.0001

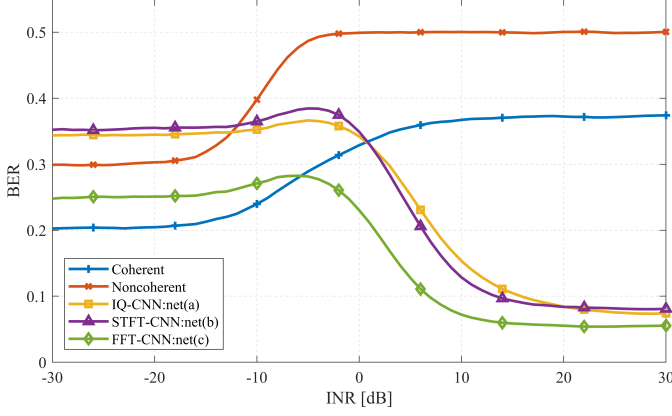


Fig. 4. detection performance for a target LoRa symbol with SF7, an interference LoRa signal with SF7, and a fixed SINR = -15dB .

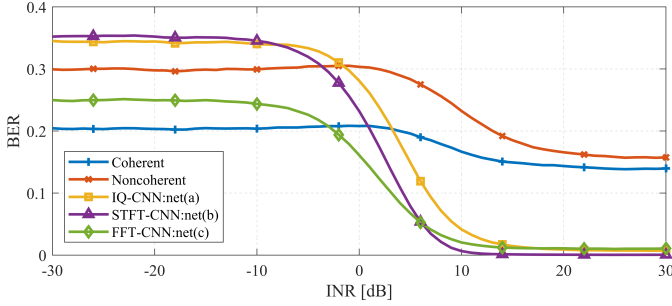


Fig. 5. detection performance for a target LoRa symbol with SF7, and an interference LoRa signal with SF8, and a fixed SINR = -15dB .

symbols long packet for HybNet is about twice the time of the FFT-CNN, which is ≈ 6.5 milliseconds.

We further explored the detection time of the different networks as the number of frames to be classified changes. The theoretical time complexity for all the networks can be expressed as $O\left(L \sum_{l=1}^M K_{l-1} F_l W_l K_l\right)$ [40], where l is the index of convolutional layers and M is the number of

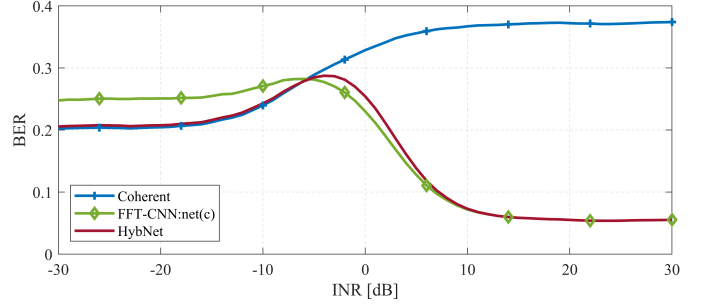


Fig. 6. detection performance of the switching architecture for a target LoRa symbol with SF = 7, an interference LoRa signal with SF = 7, and a fixed SINR = -15dB .

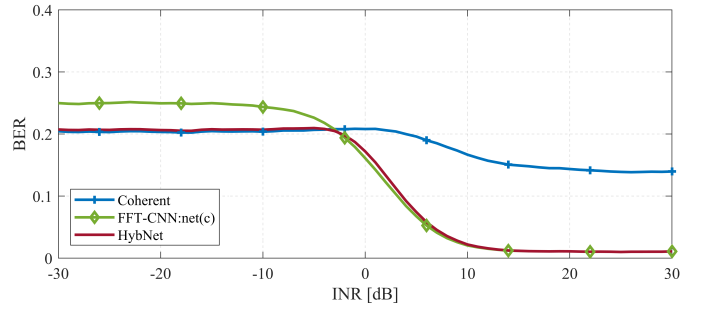


Fig. 7. detection performance of the switching architecture for a target LoRa symbol with SF = 7, an interference LoRa signal with SF = 8, and a fixed SINR = -15dB .

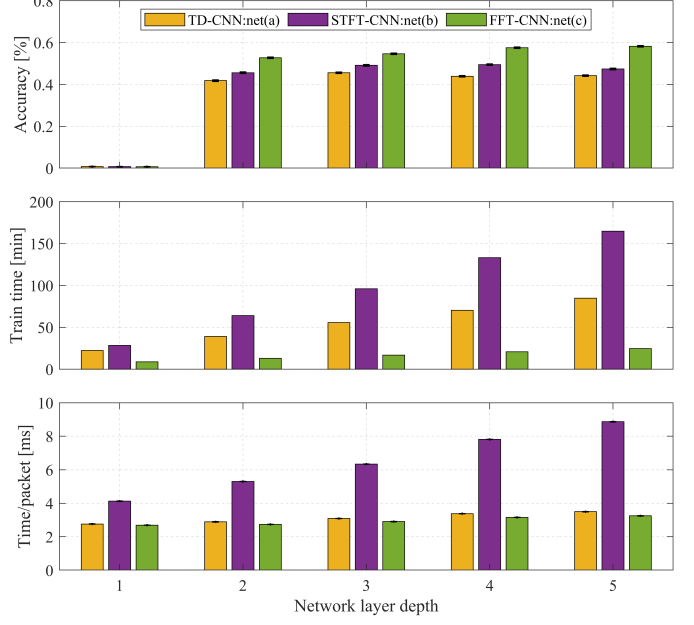


Fig. 8. Comparison of network performance in terms of network depth for classification accuracy (top plot), training time (middle plot), and time complexity per 20 symbol packet (bottom plot.) For the top and bottom plots, error bars are plotted showing the 95% confidence interval.

layers. L is the number of input symbols, K_{l-1} denotes the number of input channels. F_l is the dimensions of the convolutional filter multiplied together. W_l is the number of

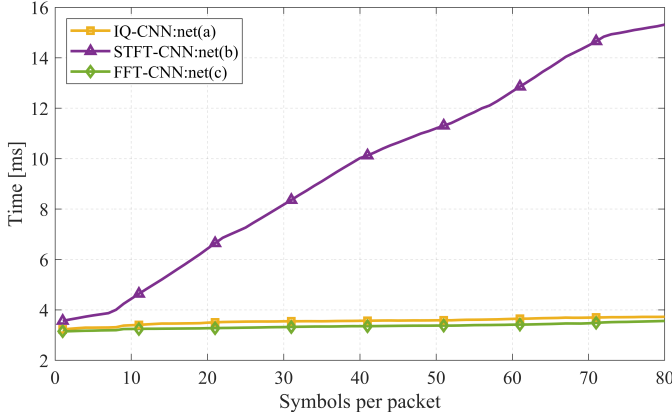


Fig. 9. The packet detection time-varying number of input symbols, comparing the three deep networks investigated in this paper.

filters per convolutional layer. Finally, K_l is the dimensions of the output multiplied together. The *max-pooling*, *dropout*, and *fully connected layers* have an insignificant time-complexity compared to the convolution layers, so their complexity is not included in the calculation. From the theoretical expression, the time-complexity linearly increases with a number of input symbols for all three networks. The theoretical expression also shows the time-complexity is much higher for the STFT-CNN since the convolutional filters F_l as well as the output dimensions K_l are 2-dimensional. This is experimentally demonstrated in Fig. 9.

VI. CONCLUSION

This paper investigated deep learning approaches that rely on convolutional neural networks for the detection of LoRa symbols in the presence of AWGN and *colored* interference. We presented a new framework *HybNet*, a switching detection architecture, which combines the merits of (i) the optimal detection in Gaussian noise based on the matched filter, with (ii) the improved performance of deep learning detector under non-Gaussian interference. We tested different input data modalities for deep learning, namely; (i) I/Q-based, (ii) time-frequency-based, and (iii) spectrum-based. The spectrum-based deep detector showed the best detection performance in heavy interference conditions and the lowest time complexity compared to the I/Q-based and time-frequency-based networks. This performance suggests that a hybrid deep learning-match filter receiver would outperform conventional detection methods in a broader range of applications, especially in random access IoT networks where the interference is caused by overlapping co-channel transmissions.

REFERENCES

- [1] Ericsson, “Ericsson Mobility Report,” *Ericsson*, Jun 2021.
- [2] B. Al Homssi, A. Al-Hourani, R. J. Evans, K. G. Chavez, S. Kandeepan, W. S. T. Rowe, and M. Loney, “Free spectrum for IoT: How much can it take?,” in *2018 IEEE International Conference on Communications Workshops (ICC Workshops)*, 2018.
- [3] M. K. Simon and M.-S. Alouini, *Digital communication over fading channels*, vol. 95. John Wiley & Sons, 2005.
- [4] LoRa Alliance, “Specification, LoRaWAN.” *LoRaWAN*, 2018. [Online]. Available: <https://lora-alliance.org/sites/default/files/2018-07/lorawan1.0.3.pdf> [Accessed: Oct. 5, 2020].
- [5] B. Vejlgaard, M. Lauridsen, H. Nguyen, I. Z. Kovacs, P. Mogensen, and M. Sorensen, “Interference impact on coverage and capacity for low power wide area IoT networks,” in *2017 IEEE Wireless Communications and Networking Conference (WCNC)*, 2017.
- [6] B. Manzoor, A. Al-Hourani, B. A. Homssi, K. Magowe, S. Kandeepan, and K. G. Chavez, “Evaluating coverage performance of NB-IoT in the ISM-band,” in *2020 27th International Conference on Telecommunications (ICT)*, 2020.
- [7] B. Al Homssi, K. Dakic, S. Maselli, H. Wolf, S. Kandeepan, and A. Al-Hourani, “IoT network design using open-source lora coverage emulator,” *IEEE Access*, vol. 9, pp. 53636–53646, 2021.
- [8] A. Mahmood, E. Sisinni, L. Guntupalli, R. Rondon, S. A. Hassan, and M. Gidlund, “Scalability analysis of a lora network under imperfect orthogonality,” *IEEE Transactions on Industrial Informatics*, vol. 15, no. 3, pp. 1425–1436, 2019.
- [9] T. Elshabrawy and J. Robert, “Analysis of ber and coverage performance of lora modulation under same spreading factor interference,” in *2018 IEEE 29th Annual International Symposium on Personal, Indoor and Mobile Radio Communications (PIMRC)*, 2018.
- [10] K. Dakic, B. Al Homssi, A. Al-Hourani, and M. Lech, “Lora signal demodulation using deep learning, a time-domain approach,” in *2021 IEEE 93rd Vehicular Technology Conference (VTC2021-Spring)*, 2021.
- [11] N. Farsad and A. Goldsmith, “Neural network detection of data sequences in communication systems,” *IEEE Transactions on Signal Processing*, vol. 66, no. 21, pp. 5663–5678, 2018.
- [12] L. Sun, Y. Wang, A. L. Swindlehurst, and X. Tang, “Generative-adversarial-network enabled signal detection for communication systems with unknown channel models,” *IEEE Journal on Selected Areas in Communications*, vol. 39, no. 1, pp. 47–60, 2021.
- [13] N. Shlezinger, N. Farsad, Yonina, and Andrea, “Viterbinet: A deep learning based viterbi algorithm for symbol detection,” *arXiv pre-print server*, 2020.
- [14] T. O’Shea and J. Hoydis, “An introduction to deep learning for the physical layer,” *IEEE Transactions on Cognitive Communications and Networking*, vol. 3, no. 4, pp. 563–575, 2017.
- [15] J. Gu, Z. Wang, J. Kuen, L. Ma, A. Shahroud, B. Shuai, T. Liu, X. Wang, G. Wang, J. Cai, and T. Chen, “Recent advances in convolutional neural networks,” *Pattern Recognition*, vol. 77, pp. 354 – 377, 2018.
- [16] Y. Wang, M. Liu, J. Yang, and G. Gui, “Data-driven deep learning for automatic modulation recognition in cognitive radios,” *IEEE Transactions on Vehicular Technology*, vol. 68, no. 4, pp. 4074–4077, 2019.
- [17] H. N. Abdullah and H. S. Abed, “Improvement of energy consumption in cognitive radio by reducing the number of sensed samples,” in *2016 Al-Sadeq International Conference on Multidisciplinary in IT and Communication Science and Applications (AIC-MITCSA)*, 2016.
- [18] T. Cover, “Broadcast channels,” *IEEE Transactions on Information Theory*, vol. 18, no. 1, pp. 2–14, 1972.
- [19] M. Aldababsa, M. Toka, S. Gökçeli, G. K. Kurt, and O. Kucur, “A tutorial on nonorthogonal multiple access for 5G and beyond,” *Wireless Communications and Mobile Computing*, vol. 2018, p. 9713450, 2018.
- [20] D. Croce, M. Guicciardo, S. Mangione, G. Santaromita, and I. Tinnirello, “Impact of lora imperfect orthogonality: Analysis of link-level performance,” *IEEE Communications Letters*, vol. 22, no. 4, pp. 796–799, 2018.
- [21] A. Waret, M. Kaneko, A. Guitton, and N. El Rachkidy, “Lora throughput analysis with imperfect spreading factor orthogonality,” *IEEE Wireless Communications Letters*, vol. 8, no. 2, pp. 408–411, 2019.
- [22] O. Afisiadis, S. Li, A. Burg, and A. Balatsoukas-Stimming, “On the advantage of coherent lora detection in the presence of interference,” *arXiv: Signal Processing*, 2020.
- [23] L. Amichi, M. Kaneko, E. H. Fukuda, N. El Rachkidy, and A. Guitton, “Joint allocation strategies of power and spreading factors with imperfect orthogonality in lora networks,” *IEEE Transactions on Communications*, vol. 68, no. 6, pp. 3750–3765, 2020.
- [24] O. Afisiadis, M. Cotting, A. Burg, and A. Balatsoukas-Stimming, “On the error rate of the lora modulation with interference,” *IEEE Transactions on Wireless Communications*, vol. 19, no. 2, pp. 1292–1304, 2020.
- [25] T. Elshabrawy and J. Robert, “Closed-form approximation of LoRa modulation ber performance,” *IEEE Communications Letters*, vol. 22, no. 9, pp. 1778–1781, 2018.
- [26] T. J. O’Shea, T. Roy, and T. C. Clancy, “Over-the-air deep learning based radio signal classification,” *IEEE Journal of Selected Topics in Signal Processing*, vol. 12, no. 1, pp. 168–179, 2018.
- [27] B. A. Homssi, A. Al-Hourani, Z. Krusevac, and W. S. T. Rowe, “Machine learning framework for sensing and modeling interference in IoT frequency bands,” *IEEE Internet of Things Journal*, pp. 1–1, 2020.

- [28] T. Gale, T. Šolc, R. Moșoi, M. Mohorčič, and C. Fortuna, “Automatic detection of wireless transmissions,” *IEEE Access*, vol. 8, pp. 24370–24384, 2020.
- [29] H. Sun, X. Chen, Q. Shi, M. Hong, X. Fu, and N. D. Sidiropoulos, “Learning to optimize: Training deep neural networks for interference management,” *IEEE Transactions on Signal Processing*, vol. 66, no. 20, pp. 5438–5453, 2018.
- [30] C. Zhang, P. Patras, and H. Haddadi, “Deep learning in mobile and wireless networking: A survey,” *IEEE Communications Surveys & Tutorials*, vol. 21, no. 3, pp. 2224–2287, 2019.
- [31] T. J. O’Shea, K. Karra, and T. C. Clancy, “Learning to communicate: Channel auto-encoders, domain specific regularizers, and attention,” in *2016 IEEE International Symposium on Signal Processing and Information Technology (ISSPIT)*, IEEE, 2016.
- [32] C. Zou, F. Yang, J. Song, and Z. Han, “Channel autoencoder for wireless communication: State of the art, challenges, and trends,” *IEEE Communications Magazine*, vol. 59, no. 5, pp. 136–142, 2021.
- [33] H. Ye, L. Liang, G. Y. Li, and B.-H. Juang, “Deep learning-based end-to-end wireless communication systems with conditional gans as unknown channels,” *IEEE Transactions on Wireless Communications*, vol. 19, no. 5, pp. 3133–3143, 2020.
- [34] H. Ye, G. Y. Li, and B.-H. Juang, “Power of deep learning for channel estimation and signal detection in ofdm systems,” *IEEE Wireless Communications Letters*, vol. 7, no. 1, pp. 114–117, 2018.
- [35] C. Liu, Y. Chen, and S.-H. Yang, “Signal detection with co-channel interference using deep learning,” *Physical Communication*, vol. 47, p. 101343, 2021.
- [36] J. Xia, K. He, W. Xu, S. Zhang, L. Fan, and G. K. Karagiannidis, “A mimo detector with deep learning in the presence of correlated interference,” *IEEE Transactions on Vehicular Technology*, vol. 69, no. 4, pp. 4492–4497, 2020.
- [37] A. Marquet, N. Montavont, and G. Z. Papadopoulos, “Investigating theoretical performance and demodulation techniques for lora,” in *2019 IEEE 20th International Symposium on “A World of Wireless, Mobile and Multimedia Networks” (WoWMoM)*, 2019.
- [38] B. Al Homssi and A. Al-Hourani, “LoRa Matlab emulator,” 2020. data retrieved from AURIN, <https://au.mathworks.com/matlabcentral/fileexchange/81166-loramatlab>.
- [39] J. Snoek, H. Larochelle, and R. P. Adams, “Practical bayesian optimization of machine learning algorithms,” in *Advances in neural information processing systems*, 2012.
- [40] K. He and J. Sun, “Convolutional neural networks at constrained time cost,” in *Proceedings of the IEEE conference on computer vision and pattern recognition*, 2015.